# On an asymptotic expansion for porous media flow of Carreau fluids


T. Götz *
Dept. of Mathematics
University of Kaiserslautern
Postbox 3049
D–67653 Kaiserslautern
Germany

H. A. Parhusip †
Dept. of Mathematics
Institut Teknologi Bandung
Jl. Ganesha 10
Bandung 40132
Indonesia


September 8, 2004


**Abstract**

Porous media flow of polymers with Carreau law viscosities and their application to enhanced oil recovery (EOR) is considered. Applying the homogenization method leads to a nonlinear two-scale problem. In case of a small difference between the Carreau and the Newtonian case an asymptotic expansion based on the small deviation of the viscosity from the Newtonian case is introduced. For uni-directional pressure gradients, which is a reasonable assumption in applications like EOR, auxiliary problems to decouple the micro- from the macrovariables are derived. The microscopic flow field obtained by the proposed approach is compared to the solution of the two-scale problem. Finite element calculations for an isotropic and an anisotropic pore cell geometries are used to validate the accuracy and speed-up of the proposed approach. The order of accuracy has been studied by performing the simulations up to the third order expansion for the isotropic geometry.


## 1 Introduction

Polymer flooding has been found to be an excellent method for improving oil recovery (EOR, Enhanced Oil Recovery). Polymers are added to the injected water to increase its viscosity and to improve the oil-water mobility ratio [1, 2]. For heavy oil with viscosities $10^3 - 10^6$ times higher than water [3], the water injection technique as described in [4, 5] is not applicable and polymer injection is used. To describe polymer flooding in porous media, engineers use the Darcy


*E–Mail: goetz@mathematik.uni-kl.de
†E–Mail: hanna_p@dns.math.itb.ac.id

filtration law and the porous medium is considered to consist of connected arrays of capillaries [6, 7, 8]. The permeability is either obtained by measurements or deduced from known models such as Kozeny-Carman [9].

However, Darcy's law and the permeability can be derived from the microscopic Stokes flow equations using homogenization techniques, which are asymptotic expansions in the small ratio $\varepsilon$ of the microscopic and the macroscopic length scale, see [10, 11] and references therein. In the Newtonian case, the micro- and macroscale decouple and one obtains a local relation between the pressure gradient and the flow velocity. The homogenization of non-Newtonian flows has been discussed in [12, 13, 14, 15]. The resulting filtration laws are in general non-local, i. e. the micro- and macroscale do not decouple. To remedy this drawback in the non-Newtonian case, numerical methods to solve the two-scale homogenized system are used [16, 17] or non-linear filtration laws have been derived, see [18, 19] and references therein. Non-Newtonian Hele-Shaw flows and their analogy to porous media equations are also widely discussed in literature, see [20, 21, 22].

The rheologic behavior of the polymeric liquids used in EOR is frequently described in engineering literature by either the power law or the Carreau law [6]. The recent development of stochastic homogenization for power-law fluids may be found in [23].

Since the concentration of the polymers is rather low, the difference between the real rheologic behavior and the Newtonian case is typically very small. This suggests to introduce a second asymptotic expansion based on the small deviation of the viscosity from the Newtonian case. For uni-directional pressure gradients, which is a reasonable assumption in applications like EOR, we derive auxiliary problems to decouple the micro- from the macrovariables.

According to the power law (sometimes also called Ostwald-de Waele law), the viscosity is given by

$$\eta = \eta(\gamma) = \lambda\,\gamma^{r-2}\ , \tag{1}$$

where $\gamma = \|\mathrm{D}\boldsymbol{u}\| = \left(\sum_{i,j}(\mathrm{D}_{i,j}\boldsymbol{u})^2\right)^{1/2}$ denotes the shear rate and the rate-of-strain tensor is given by $\mathrm{D}\boldsymbol{u} = \frac{1}{2}\left[\nabla\boldsymbol{u} + \nabla\boldsymbol{u}^\top\right]$. The parameters $\lambda$ and $r$ are called the consistency and the flow index. The flow index $r$ characterizes the fluid: For $r > 2$ the fluid is called dilatant, $r = 2$ corresponds to Newtonian behavior, the range $1 < r < 2$ is called pseudo plastic and $r = 1$ yields purely plastic flows. We focus in this paper on the pseudo plastic regime, i. e. $r \in (1, 2)$. Due to its simplicity and ability to fit experimental viscosity data for a large class of fluids, this model is very popular. However, one disadvantage of the power law is, that it does not accurately describe the behavior of the viscosity for low shear rates. According to the power law, the viscosity tends to infinity for low shear rates and $r \in (1, 2)$, whereas for real fluids it tends to some constant value $\eta_0$ called the zero-shear-rate viscosity. Hence, we consider as a generalization the Carreau law:

$$\eta = \eta(\gamma) = (\eta_0 - \eta_\infty)\left(1 + \lambda\gamma^2\right)^{r/2-1} + \eta_\infty\ ,$$

where $\eta_0 > \eta_\infty > 0,\ \lambda > 0,\ 1 < r < 2$. The parameter $\lambda$ is a time constant, $r$ is a dimensionless constant describing the slope in the power law region and $\eta_\infty$ is the high shear rate limit of the viscosity.

Scaling the spatial coordinates with a typical length $L$ and the velocities with a typical velocity $U$, we obtain the non-dimensional Carreau law of the form

$$\tilde{\eta} = (\tilde{\eta}_0 - \tilde{\eta}_\infty)\left(1 + \tilde{\lambda}\tilde{\gamma}^2\right)^{r/2-1} + \tilde{\eta}_\infty\ , \tag{2}$$

where $\tilde{\eta} = \eta/\eta_R$ is the non-dimensional viscosity, $\eta_R$ some reference value for the viscosity, $\tilde{\lambda} = (U/L)^2\lambda$ is a dimensionless parameter and $\tilde{\gamma} = (L/U)\gamma$ denotes the non-dimensional shear rate. In the sequel we will always work with this non-dimensional form of the Carreau law and skip the tilde.

Most of the flows involved in polymer processing are slow. Therefore we consider only creeping flow, i. e. low-Reynolds number flows, neglecting inertial effects.

Although we consider throughout this paper only two-dimensional flows, the proposed method can be generalized to three-dimensional situations. However, the numerical simulations get more involved and require special attention to keep the computational efforts within reasonable limits.

This paper is organized as follows. In Section 2 we review the formal homogenization of non-Newtonian flows where the viscosity is modeled by a power or Carreau law. Assuming the porous medium to consist of a periodic arrangement of cells with size $\varepsilon$, we use a two-scale power series ansatz for the velocity and the pressure. If the rheologic parameter $\lambda$ in the Carreau law is also small, we introduce in Section 3 a second power series with respect to this parameter. This will lead us to a sequence of cell problems similar to the Newtonian case. Section 4 presents numerical simulations to illustrate the accuracy of the proposed asymptotic approach.

Throughout this paper we use boldface italic letters for vectors (e. g. $\boldsymbol{u} \in \mathbb{R}^2$) and boldface upright letters for matrices (e. g. $\mathbf{D} \in \mathbb{R}^{2\times 2}$).

## 2 Non-Newtonian porous media flow

We consider a porous medium $\Omega \subset \mathbb{R}^2$ with a typical dimension $L_{\boldsymbol{x}}$ and call $\boldsymbol{x} \in \Omega$ the macrovariable. We assume that $\Omega$ consists of a periodic repetition of an elementary square cell $\mathcal{Y}^\varepsilon$ of size $L_{\boldsymbol{y}} = \varepsilon L_{\boldsymbol{x}}$, where $\varepsilon \ll 1$. This elementary cell contains the fluid part $\mathcal{F}^\varepsilon \subset \mathcal{Y}^\varepsilon$ and the solid part $\mathcal{S}^\varepsilon = \overline{\Omega \backslash \mathcal{F}^\varepsilon}$, see Figure 1.

On the elementary cell we consider the non-dimensional, incompressible Stokes equations given by

$$\varepsilon^2 \nabla \cdot [\eta^\varepsilon\, \mathrm{D}\boldsymbol{u}^\varepsilon] = \nabla p^\varepsilon \qquad \text{in } \mathcal{F}^\varepsilon\ , \tag{3a}$$

$$\nabla \cdot \boldsymbol{u}^\varepsilon = 0 \qquad \text{in } \mathcal{F}^\varepsilon\ , \tag{3b}$$

$$\boldsymbol{u}^\varepsilon = 0 \qquad \text{on } \partial\mathcal{S}^\varepsilon\ . \tag{3c}$$

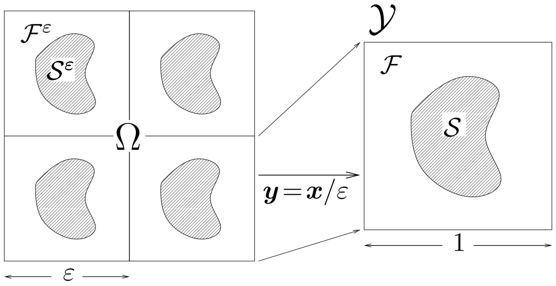


Figure 1: Sketch of the considered geometry. Note that both the macrovariable $\boldsymbol{x}$ and the microvariable $\boldsymbol{y}$ are vectors in $\mathbb{R}^2$.

Analogously to the Newtonian case [10], we introduce the microvariable $\boldsymbol{y} = \boldsymbol{x}/\varepsilon \in \mathbb{R}^2$ defined on the upscaled elementary cell $\mathcal{Y}$ (with fluid part $\mathcal{F}$ and solid part $\mathcal{S}$) and assume the following two-scale asymptotic expansions for the velocity $\boldsymbol{u}^\varepsilon$ and the pressure $p^\varepsilon$

$$\begin{aligned}\boldsymbol{u}^\varepsilon(\boldsymbol{x}) = \boldsymbol{u}^\varepsilon(\boldsymbol{x},\boldsymbol{y}) &= \boldsymbol{u}_0(\boldsymbol{x},\boldsymbol{y}) + \varepsilon\boldsymbol{u}_1(\boldsymbol{x},\boldsymbol{y}) + \varepsilon^2\boldsymbol{u}_2(\boldsymbol{x},\boldsymbol{y}) + \dots\ ,\\ p^\varepsilon(\boldsymbol{x}) = p^\varepsilon(\boldsymbol{x},\boldsymbol{y}) &= p_0(\boldsymbol{x},\boldsymbol{y}) + \varepsilon p_1(\boldsymbol{x},\boldsymbol{y}) + \varepsilon^2 p_2(\boldsymbol{x},\boldsymbol{y}) + \dots\ ,\end{aligned}$$

where the coefficient functions $\boldsymbol{u}_i$ and $p_i$ are $\boldsymbol{y}$–periodic. We expand the rate-of-strain tensor $\mathrm{D}\boldsymbol{u}^\varepsilon$ as

$$\mathrm{D}\boldsymbol{u}^\varepsilon(\boldsymbol{x}) = \mathrm{D}\boldsymbol{u}^\varepsilon(\boldsymbol{x},\boldsymbol{y}) = \varepsilon^{-1}\mathbf{d}_{-1}(\boldsymbol{x},\boldsymbol{y}) + \mathbf{d}_0(\boldsymbol{x},\boldsymbol{y}) + \varepsilon\mathbf{d}_1(\boldsymbol{x},\boldsymbol{y}) + \dots\ ,$$

where $\mathbf{d}_{-1} = \mathrm{D}_{\boldsymbol{y}}\boldsymbol{u}_0 = \frac{1}{2}\left[\nabla_{\boldsymbol{y}}\,\boldsymbol{u}_0 + \nabla_{\boldsymbol{y}}\,\boldsymbol{u}_0^\top\right]$, $\mathbf{d}_0 = \mathrm{D}_{\boldsymbol{x}}\boldsymbol{u}_0 + \mathrm{D}_{\boldsymbol{y}}\boldsymbol{u}_1$ and $\mathbf{d}_1 = \mathrm{D}_{\boldsymbol{x}}\boldsymbol{u}_1 + \mathrm{D}_{\boldsymbol{y}}\boldsymbol{u}_2$.

For a large class of non-Newtonian media, the generalized viscosity $\eta^\varepsilon$ is given as a function of the shear rate $\gamma^2 = \|\mathrm{D}\boldsymbol{u}^\varepsilon\|_2^2$. Expanding the shear rate in terms of $\varepsilon$ yields

$$\gamma^2 = \varepsilon^{-2}\gamma_{-2} + \varepsilon^{-1}\gamma_{-1} + \gamma_0 + \dots\ ,$$

where $\gamma_{-2} = \|\mathbf{d}_{-1}\|_2^2$, $\gamma_{-1} = 2\,\mathrm{tr}\,(\mathbf{d}_{-1}\,\mathbf{d}_0)$ and $\gamma_0 = \|\mathbf{d}_0\|_2^2 + 2\,\mathrm{tr}\,(\mathbf{d}_{-1}\,\mathbf{d}_1)$, since all the $\mathbf{d}_i$ are symmetric. Now, the viscosity function $\eta^\varepsilon = \eta(\varepsilon^2\gamma^2)$ can also be written in terms of $\varepsilon$

$$\eta^\varepsilon = \eta_0 + \varepsilon\eta_1 + \varepsilon^2\eta_2 + \dots\ ,$$

where $\eta_0 = \eta(\gamma_{-2})$, $\eta_1 = \eta'(\gamma_{-2})\gamma_{-1}$ and $\eta_2 = \eta'(\gamma_{-2})\gamma_0 + \eta''(\gamma_{-2})\gamma_{-1}^2/2$.

Plugging the above expansions into (3) and collecting equal powers of $\varepsilon$ yields

$$\nabla_{\boldsymbol{y}}\,p_0 = 0 \qquad\qquad \text{for } \boldsymbol{y} \in \mathcal{Y}\ . \tag{4}$$

Hence $p_0 = p_0(\boldsymbol{x})$, i. e. the leading order $p_0$ of the pressure is independent of the microvariable $\boldsymbol{y}$. The next order terms lead to the *two-scale problem*

$$
\begin{aligned}
\nabla_{\boldsymbol{y}} \cdot [\eta(\gamma_{-2})\, \mathbf{d}_{-1}] &= \nabla_{\boldsymbol{x}}\, p_0 + \nabla_{\boldsymbol{y}}\, p_1 && \text{in } \Omega \times \mathcal{F} \;, && \text{(5a)}\\
\nabla_{\boldsymbol{y}} \cdot \boldsymbol{u}_0 &= 0 && \text{in } \Omega \times \mathcal{F} \;, && \text{(5b)}\\
\boldsymbol{u}_0 &= 0 && \text{on } \Omega \times \partial\mathcal{S} \;, && \text{(5c)}\\
(\boldsymbol{u}_0, p_1) & \quad \text{is } \boldsymbol{y}\text{-periodic} && \text{on } \Omega \;, && \text{(5d)}
\end{aligned}
$$

and $\nabla_{\boldsymbol{x}} \cdot \boldsymbol{u}^{\varepsilon} = 0$ as well as the $\boldsymbol{y} -$ *periodicity* yield

$$
\nabla_{\boldsymbol{x}} \cdot \int_{\mathcal{Y}} \boldsymbol{u}_0 \, d\boldsymbol{y} = 0 \qquad \text{on } \Omega \;. \tag{5e}
$$

In [10], existence and uniqueness results for problem (5) and Carreau or power law viscosities are given. Some of the importance of the two-scale asymptotic expansions applied to Newtonian flow in porous media arises from the fact that, for Newtonian fluids the above two-scale problem (5) separates the macro- and microvariable. Hence, one can derive so-called auxiliary problems, that depend solely on the $\boldsymbol{y}$-variable and that can be used to define a permeability tensor.

## 2.1 Derivation of auxiliary problems

In the Newtonian case, Equation (5a) is linear and reads as $\eta \triangle_{\boldsymbol{y}} \boldsymbol{u}_0 = \nabla_{\boldsymbol{x}}\, p_0 + \nabla_{\boldsymbol{y}}\, p_1$. Rewriting $\nabla_{\boldsymbol{x}}\, p_0$ componentwise we introduce the *auxiliary problem*

$$
\triangle_{\boldsymbol{y}} \boldsymbol{w}_k = \boldsymbol{e}_k + \nabla_{\boldsymbol{y}}\, \pi_k \;, \tag{6}
$$

where $\boldsymbol{w}_k(\boldsymbol{y})$ and $\pi_k(\boldsymbol{y})$ depend solely on the microvariable. The solution $\boldsymbol{u}_0(\boldsymbol{x}, \boldsymbol{y})$ and $p_1(\boldsymbol{x}, \boldsymbol{y})$ of (5) is then given by

$$
\begin{aligned}
\boldsymbol{u}_0(\boldsymbol{x}, \boldsymbol{y}) &= \frac{1}{\eta} \sum_k \partial_k\, p_0(\boldsymbol{x}) \cdot \boldsymbol{w}_k(\boldsymbol{y}) \;,\\
p_1(\boldsymbol{x}, \boldsymbol{y}) &= \sum_k \partial_k\, p_0(\boldsymbol{x}) \cdot \pi_k(\boldsymbol{y}) \;.
\end{aligned}
$$

Averaging over the microvariable $\boldsymbol{y}$ we obtain *Darcy's law*

$$
\boldsymbol{u}_0(\boldsymbol{x}) = \int_{\mathcal{Y}} \boldsymbol{u}_0(\boldsymbol{x}, \boldsymbol{y}) \; d\boldsymbol{y} = \frac{1}{\eta} \sum_k \partial_k\, p_0(\boldsymbol{x}) \int_{\mathcal{Y}} \boldsymbol{w}_k(\boldsymbol{y}) \; d\boldsymbol{y} =: \frac{\mathbf{M}}{\eta} \cdot \nabla p_0 \;,
$$

where $\mathbf{M}$ is the permeability tensor.

To generalize this approach to the non-Newtonian case and to find conditions for the existence of decoupled auxiliary problems, we propose the ansatz

$$
\boldsymbol{u}_0(\boldsymbol{x}, \boldsymbol{y}) = \sum_k f(\partial_k\, p_0) \cdot \boldsymbol{w}_k(\boldsymbol{y}) \;, \tag{7a}
$$

$$
p_1(\boldsymbol{x}, \boldsymbol{y}) = \sum_k g(\partial_k\, p_0) \cdot \pi_k(\boldsymbol{y}) \;, \tag{7b}
$$

where $f$ and $g$ are some yet arbitrary functions. Plugging this ansatz for $\boldsymbol{u}_0$ into the shear rate we obtain

$$\begin{aligned}\gamma_{-2}(\boldsymbol{x},\boldsymbol{y}) &= \sum_k f(\partial_k\, p_0)^2\, \|\mathrm{D}\boldsymbol{w}_k\|_2^2 \\ &\quad + \sum_{k\neq l} f(\partial_k\, p_0) f(\partial_l\, p_0)\, \mathrm{tr}\left(\mathrm{D}\boldsymbol{w}_k\, \mathrm{D}\boldsymbol{w}_l + \mathrm{D}\boldsymbol{w}_l\, \mathrm{D}\boldsymbol{w}_k\right)\ , \end{aligned} \tag{8}$$

and hence the two-scale problem (5a) reads as

$$\begin{aligned}&\sum_k f(\partial_k\, p_0)\ \nabla_{\boldsymbol{y}} \cdot \left[(\eta_0(\boldsymbol{x},\boldsymbol{y})\, \mathrm{D}\boldsymbol{w}_k(\boldsymbol{y})\right] \\ &\qquad = \sum_k \partial_k\, p_0(\boldsymbol{x}) \cdot \boldsymbol{e}_k + \sum_k g(\partial_k\, p_0) \cdot \nabla_{\boldsymbol{y}} \pi_k(\boldsymbol{y})\ . \end{aligned} \tag{9}$$

If the viscosity function separates like $\eta_0(\boldsymbol{x},\boldsymbol{y}) = \varphi(\boldsymbol{x})\, \psi(\boldsymbol{y})$, we can derive an auxiliary problem similar to (6) depending solely on the microvariable $\boldsymbol{y}$.

Let us restrict to the case of an uni-directional gradient of the macroscopic pressure, i. e. $\partial_k\, p_0 = 0$ for all but one $k$. This assumption is quite realistic in applications like EOR, since the microscopic flow is driven mainly by the pressure difference between the injection point and the well. In this flow regime, the expression for the shear rate (8) simplifies to

$$\gamma_{-2}(\boldsymbol{x},\boldsymbol{y}) = f(\partial_k\, p_0(\boldsymbol{x}))^2\, \|\mathrm{D}\boldsymbol{w}_k(\boldsymbol{y})\|_2^2 = \tilde{f}(\boldsymbol{x})\, \tilde{\gamma}(\boldsymbol{y})\ . \tag{10}$$

To obtain an auxiliary problem, it is required that

$$\eta(\gamma_{-2}) = \eta\left(\tilde{f}(\boldsymbol{x})\, \tilde{\gamma}(\boldsymbol{y})\right) = \varphi(\boldsymbol{x})\, \psi(\boldsymbol{y})\ . \tag{11}$$

Considering $\partial_{\boldsymbol{y}}\left(\partial_{\boldsymbol{x}}\,(11)/(11)\right)$ and introducing $z = \tilde{f}(\boldsymbol{x})\, \tilde{\gamma}(\boldsymbol{y})$ we obtain the differential equation

$$\frac{\eta\eta'' - {\eta'}^2}{\eta^2} z + \frac{\eta'}{\eta} = 0 \qquad \Longrightarrow \qquad (\log\eta)''\, z + (\log\eta)' = 0$$

for $\eta = \eta(z)$ with the general solution

$$\eta(z) = c_1 z^n\ .$$

Hence, in case of an uni-directional macroscopic pressure gradient we can expect auxiliary problems only for Newtonian ($n = 0$) or power-law fluids ($n \neq 0$).

## 2.2 Power-law fluids

For a power-law fluid, the viscosity is given by (1). Using (10) we obtain $\eta_0 = \lambda\, f(\partial_k\, p_0(\boldsymbol{x}))^{r-2}\, \|\mathrm{D}\boldsymbol{w}_k(\boldsymbol{y})\|_2^{r-2}$ for the leading term of the viscosity. The two-scale problem (5a) reads as

$$\begin{aligned}&\lambda\, f(\partial_k\, p_0)^{r-1}\ \nabla_{\boldsymbol{y}} \cdot \left(\|\mathrm{D}\boldsymbol{w}_k(\boldsymbol{y})\|_2^{r-1}\ \mathrm{D}\boldsymbol{w}_k(\boldsymbol{y})\right) \\ &\qquad = \partial_k\, p_0(\boldsymbol{x}) \cdot \boldsymbol{e}_k + g(\partial_k\, p_0) \cdot \nabla_{\boldsymbol{y}}\, \pi_k(\boldsymbol{y})\ . \end{aligned}$$

Setting $f(\partial_k p_0) = (\partial_k p_0)^{1/(r-1)}$ and $g(\partial_k p_0) = \partial_k p_0$ yields the following auxiliary problem, independent of the macrovariable $\boldsymbol{x}$,

$$\nabla_{\boldsymbol{y}} \cdot \Big( \|\mathrm{D}\boldsymbol{w}_k(\boldsymbol{y})\|_2^{r-1} \ \mathrm{D}\boldsymbol{w}_k(\boldsymbol{y}) \Big) = \boldsymbol{e}_k + \nabla_{\boldsymbol{y}} \, \pi_k(\boldsymbol{y}) \qquad \text{for } \boldsymbol{y} \in \mathcal{F} \ . \tag{12}$$

Once having the solution $\boldsymbol{w}_k(\boldsymbol{y})$, we can compute the zeroth-order approximation of the velocity field

$$\boldsymbol{u}_0(\boldsymbol{x}, \boldsymbol{y}) = (\partial_k \, p_0(\boldsymbol{x}))^{1/(r-1)} \ \boldsymbol{w}_k(\boldsymbol{y}) \tag{13}$$

and averaging over the microvariable $\boldsymbol{y}$ yields the macroscopic seapage velocity

$$\tilde{\boldsymbol{u}}(\boldsymbol{x}) = (\partial_k \, p_0(\boldsymbol{x}))^{1/(r-1)} \int_{\mathcal{Y}} \boldsymbol{w}_k(\boldsymbol{y}) \, d\boldsymbol{y} \ . \tag{14}$$

Note, that this derivation is only valid in the case of a uni-directional pressure gradient. Unlike in the Newtonian case, it is not possible to construct the velocity field for arbitrary pressure gradients via superposition.

## 2.3 Carreau fluids

Using the Carreau model (2) for the viscosity we cannot construct an auxiliary problem, even not in the case of a uni-directional macroscopic pressure gradient. If $\partial_k \, p_0 = \boldsymbol{a} = \text{const.}$, we can plug (13) into (5a) and obtain the auxiliary problem

$$\nabla_{\boldsymbol{y}} \cdot \Big[ \eta(\|\mathrm{D}\boldsymbol{w}_k(\boldsymbol{y})\|_2^2) \ \mathrm{D}\boldsymbol{w}_k(\boldsymbol{y}) \Big] = \boldsymbol{a} + \nabla_{\boldsymbol{y}} \, \pi_k(\boldsymbol{y}) \qquad \text{for } \boldsymbol{y} \in \mathcal{F} \ , \tag{15}$$

with

$$\eta \left( \|\mathrm{D}\boldsymbol{w}_k(\boldsymbol{y})\|_2^2 \right) = (\eta_0 - \eta_\infty) \left( \xi_1 + \lambda \, \|\mathrm{D}\boldsymbol{w}_k(\boldsymbol{y})\|_2^2 \right)^{(\frac{r}{2}-1)} + \xi_2 \ , \tag{16}$$

and $\xi_1 = (\partial_k \, p_0(\boldsymbol{x}))^{\frac{1}{1-r}}$, $\xi_2 = \eta_\infty (\partial_k \, p_0(\boldsymbol{x}))^{-(\frac{r-2}{r-1})}$. Note, that the auxiliary problem (15) is independent of the macroscale. The microscopic velocity $w_k(\boldsymbol{y}) = \boldsymbol{w}_k(\boldsymbol{a}; \boldsymbol{y})$ depends on the pressure gradient $\boldsymbol{a}$ and averaging over the cell we obtain the macroscopic velocity

$$\tilde{\boldsymbol{u}} = \int_{\mathcal{Y}} \boldsymbol{w}_k(\boldsymbol{a}; \boldsymbol{y}) \, d\boldsymbol{y} = \tilde{\boldsymbol{u}}(\boldsymbol{a}) \ . \tag{17}$$

This equation, relating the macroscopic pressure gradient $\boldsymbol{a}$ to the seapage velocity $\boldsymbol{u}$, can be viewed as non-linear filtration law, extending Darcy's law from the Newtonian to the non-Newtonian regime.

However, we will not pursue this approach but rather focus on the rheologic parameter $\lambda$ in the Carreau law. An expansion with respect to this parameter will enable us to derive a sequence of Newtonian two-scale problems approximating (5). For each of these Newtonian problems we have the auxiliary problem available separating the macro- and microscale.

# 3 Asymptotic expansion of the Carreau model

In this section we consider the two-scale problem (5) with a viscosity given by the Carreau law (2). In the case of a small rheologic parameter $\lambda \ll 1$, we introduce a second power series for the velocity and pressure with respect to $\lambda$. For the sake of simplicity we are satisfied with an expansion up to first order terms. To obtain the higher order corrections is a straightforward but tedious algebraic exercise.

The viscosity introducing the nonlinearity in (5a) is given by

$$\eta(\gamma_{-2}) = (\eta_0 - \eta_\infty)\left(1 + \lambda \left\|\mathbf{d}_{-1}\right\|_2^2\right)^{(r/2-1)} + \eta_\infty \; .$$

Expanding with respect to $\lambda$ up to first order we obtain

$$\eta \approx \eta^{(0)} + \lambda\eta^{(1)} = \eta_0 + \lambda(\eta_0 - \eta_\infty)\left(\frac{r}{2} - 1\right)\left\|\mathbf{d}_{-1}\right\|_2^2 \; . \tag{18}$$

Note, that this power series in $\lambda$ is an expansion at zero shear rates. This type of expansion is reasonable in EOR, since the viscosity of the polymer-water mixture just slightly differs from the Newtonian viscosity of the water.

Assuming the existence of power series in $\lambda$ for $p_0(\boldsymbol{x})$ and the two-scale pressure $p_1(\boldsymbol{x}, \boldsymbol{y})$, we introduce the following ansatz for the velocity

$$\begin{aligned} \boldsymbol{u}_0(\boldsymbol{x}, \boldsymbol{y}) &= \boldsymbol{u}_0^{(0)}(\boldsymbol{x}, \boldsymbol{y}) + \lambda \boldsymbol{u}_0^{(1)}(\boldsymbol{x}, \boldsymbol{y}) \\ &= \boldsymbol{w}_k^{(0)}(\boldsymbol{y})\, g(\partial_k\, p_0)^{(0)} + \lambda \boldsymbol{w}_k^{(1)}(\boldsymbol{y})\, g(\partial_k\, p_0)^{(1)} + \dots \; . \end{aligned} \tag{19}$$

with $g(\partial_k\, p_0)^{(0)} = \partial_k\, p_0$ and $g(\partial_k\, p_0)^{(1)} = \left|\partial_k\, p_0\right|^2 \partial_k\, p_0$.

The auxiliary problem at $\mathcal{O}(\lambda^0)$ reads as

$$\begin{aligned} \eta_0 \triangle_{\boldsymbol{y}}\, \boldsymbol{w}_k^{(0)}(\boldsymbol{y}) &= \nabla_{\boldsymbol{y}}\, \pi_k^{(0)}(\boldsymbol{y}) - \boldsymbol{e}_k && \text{for } \boldsymbol{y} \in \mathcal{F} \; , \\ \nabla_{\boldsymbol{y}} \cdot \boldsymbol{w}_k^{(0)}(\boldsymbol{y}) &= 0 && \text{for } \boldsymbol{y} \in \mathcal{F} \; , \\ \boldsymbol{w}_k^{(0)}(\boldsymbol{y}) &= 0 && \text{for } \boldsymbol{y} \in \partial\mathcal{S} \; , \\ \left(\boldsymbol{w}_k^{(0)}, \pi_k^{(0)}\right) & \quad \text{is periodic in } \boldsymbol{y} \; . \end{aligned} \tag{20}$$

In the next order $\mathcal{O}(\lambda^1)$ the auxiliary problem is given by

$$\begin{aligned} \eta_0 \triangle_{\boldsymbol{y}}\, \boldsymbol{w}_k^{(1)}(\boldsymbol{y}) &= \nabla_{\boldsymbol{y}}\, \pi_k^{(1)}(\boldsymbol{y}) - \boldsymbol{e}_k + \boldsymbol{f}(\boldsymbol{w}_k^{(0)}) && \text{for } \boldsymbol{y} \in \mathcal{F} \; , \\ \nabla_{\boldsymbol{y}} \cdot \boldsymbol{w}_k^{(1)}(\boldsymbol{y}) &= 0 && \text{for } \boldsymbol{y} \in \mathcal{F} \; , \\ \boldsymbol{w}_k^{(1)}(\boldsymbol{y}) &= 0 && \text{for } \boldsymbol{y} \in \partial\mathcal{S} \; , \\ \left(\boldsymbol{w}_k^{(1)}, \pi_k^{(1)}\right) & \quad \text{is periodic in } \boldsymbol{y} \; , \end{aligned} \tag{21}$$

where

$$\boldsymbol{f}(\boldsymbol{w}_k^{(0)}) = -(\eta_0 - \eta_\infty)\left(\frac{r}{2} - 1\right)\nabla_{\boldsymbol{y}}\left(\left\|\mathrm{D}\boldsymbol{w}_k^{(0)}(\boldsymbol{y})\right\|^2 \mathrm{D}\boldsymbol{w}_k^{(0)}(\boldsymbol{y})\right) \; . \tag{22}$$

Generally we have to solve on each order $\mathcal{O}(\lambda^j)$ a Newtonian auxiliary problem of the form

$$\begin{aligned} \eta_0 \triangle_{\boldsymbol{y}} \boldsymbol{w}_k(\boldsymbol{y}) &= \nabla_{\boldsymbol{y}} \pi_k + \boldsymbol{f} && \text{in } \mathcal{F} , \\ \nabla_{\boldsymbol{y}} \cdot \boldsymbol{w}_k(\boldsymbol{y}) &= 0 && \text{in } \mathcal{F} , \\ \boldsymbol{w}_k(\boldsymbol{y}) &= 0 && \text{on } \partial\mathcal{S} , \\ (\boldsymbol{w}_k, \pi_k) & \quad \text{is periodic in } \boldsymbol{y} . \end{aligned} \tag{23}$$

Note, that having the solution $(\boldsymbol{w}_k^{(j)},\ \pi_k^{(j)})$ available, we can advance to the next order $j+1$ and get successively the contributions to compute the velocity $\boldsymbol{u}_0$ according to (19).

# 4 Simulations

In this section we show some numerical simulations to illustrate the accuracy and speed-up of the asymptotic approach presented in Section 3. We consider a range of parameters that is typical for polymers used in EOR and show two example geometries for the elementary cell representing a simplified "standard" geometry in homogenization theory as well as a more realistic geometry.

## 4.1 Geometry and parameters

We consider two different problems, an isotropic and an anisotropic porous medium. In the case of the isotropic medium, the cell $\mathcal{Y}$ is defined as a unit square $[0,1]^2$ with a centered circular inclusion of radius $R = 0.15$, see Figure 2(left). For the anisotropic problem we consider the geometry shown in Figure 2(right) serving as a quite realistic example for natural porous media [24]. The number of triangles ($NT$) and nodes ($NN$) used in the meshes for the isotropic and anisotropic geometry are listed in Table 1.

Table 1: Parameters of the triangulations used for the isotropic and anisotropic cell geometry.

| | Isotropic cell | | | Anisotropic cell | | |
|---|---|---|---|---|---|---|
| | coarse | medium | fine | coarse | medium | fine |
| $NT$ | 580 | 764 | 1360 | 3672 | 9181 | 22212 |
| $NN$ | 326 | 424 | 742 | 2194 | 5165 | 12209 |

The parameters used in the simulations are based on the data collected by Hilfer, see [25].

- Typical pore sizes in oil reservoirs are $L_{\boldsymbol{y}} \approx 10^{-4}\,\mathrm{m}$.
- Microscopic fluid velocities for reservoir flooding are $U \approx 3 \times 10^{-6}\,\mathrm{m\,s^{-1}}$.

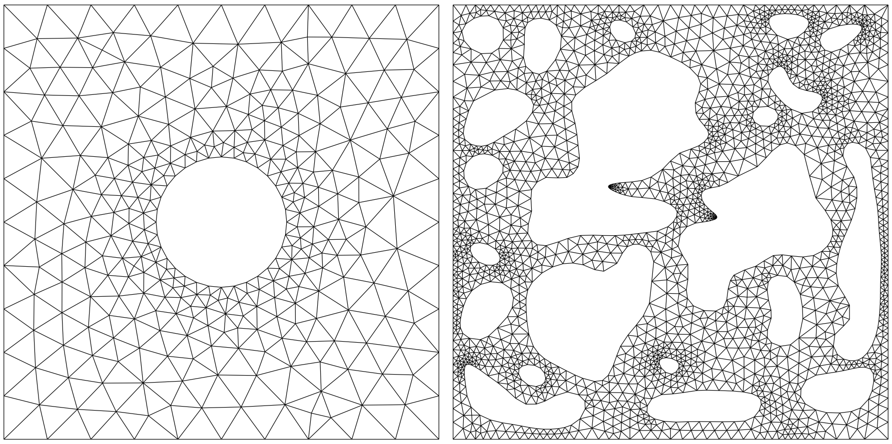

Figure 2: (left): Mesh for the isotropic cell using 580 triangles (denoted as coarse).
(right): Mesh for the anisotropic cell using 3672 triangles (denoted as coarse).

- The distance between the injection and production well is about $L_{\boldsymbol{x}} \approx 100\,\mathrm{m}$.

Hence, the ratio between the microscopic and macroscopic reference length is given by $\varepsilon = L_{\boldsymbol{y}}/L_{\boldsymbol{x}} = 10^{-6}$. This small ratio $\varepsilon$ serves as the expansion parameter in the homogenization. Concerning the macroscopic pressure $p_0$, we assume a nonzero pressure gradient in the horizontal $\boldsymbol{e}_1$ direction and a zero pressure gradient in the vertical $\boldsymbol{e}_2$ direction.

For the rheologic properties of the polymer we refer to the measurements for polymers in capillary pipes given in [26].

- Density $\rho = 1000\,\mathrm{kg\,m^{-3}}$,
- Parameters in the Carreau model: $\eta_\infty = 0.001\,\mathrm{Pa\,s}$, $\eta_0 = 0.01\,\mathrm{Pa\,s}$, $r = 1.3$, $\lambda = 0.01\,\mathrm{s}^2$.

These data yield a Reynolds number $Re = (\rho U L_{\boldsymbol{y}})/\eta_0 = 3 \times 10^{-5}$ and a dimensionless rheologic parameter $\tilde{\lambda} = \lambda\, U^2/L_{\boldsymbol{y}}^2 = 9 \times 10^{-6}$. Since $\tilde{\lambda} \ll 1$, we can use the asymptotic expansion proposed in Section 3.

As already mentioned in the Introduction, for most polymer solutions and polymer melts, the value of $r$ in the Carreau law varies between 1 and 2, see also [6]. Therefore we consider in our numerical simulations $r = 1.3$, 1.5, 1.7 and 1.9. All the numerical simulations are carried out for the dimensionless equations.

## 4.2 Solution method

The solution of the nonlinear two-scale problem (5) is considered to be exact. To solve this problem we use a Lagrangian method. Here, the idea is to view the incompressibility condition $\nabla_{\boldsymbol{y}} \cdot \boldsymbol{u}_0 = 0$ as a constraint with the pressure $p_1$ as Lagrangian multiplier. The resulting saddle point problem is discretized by finite elements using quadratic Lagrangian elements for the velocity and linear Lagrangian elements for the pressure. A detailed description of this method applied to nonlinear Stokes problems can be found in [16, 27, 28, 29].

In our numerical simulations based on the asymptotic expansion, we first solve the Problems (20) and (21) which are linear Stokes problems and use Equation (19) to obtain the velocity field.

The general outline of the numerical simulation can be summarized in the following steps:

1. Given $\partial_k p(\boldsymbol{x})$, solve Problem (20).
2. Using this solution, compute $\boldsymbol{f}$ by (22) and solve Problem (21).
3. Equation (19) yields the velocity field $\boldsymbol{u}_0(\boldsymbol{x}, \boldsymbol{y})$.
4. Use the solution of (20) as an initial guess to solve the nonlinear Problem (5).

Solving the nonlinear two-scale Stokes problem is rather expensive; hence the above proposed asymptotic procedure might provide a possible speed-up. In Table 2 the speed-up factors of the asymptotic expansion method are listed. Note, that we normalize the execution time of the nonlinear two-scale problem to 1 and that both methods are implemented using FEMLAB® 2.3.

The asymptotic expansion is found to provide a speed-up factor between 1.5 and 2 for the isotropic case and between 1.5 and 3.5 for the anisotropic geometry. One explanation for the rather fast convergence of the non-linear direct solution might be the fact, that the zeroth-order of the asymptotic expansion is used as an initial guess for the nonlinear solver. Hence the direct solution requires only a few iterations, especially in the case of $r$ large since in this case the viscosity is close to Newtonian.

## 4.3 Numerical results

### 4.3.1 First-order approximation

We have computed the velocity field inside the isotropic cell using either the full nonlinear Stokes problem (5) (here referred as *"Exact"*) and the zeroth order solution according to Problem (20) (*"Newtonian"*) and including the first order correction (21) (*"Asymptotic"*). The simulations are carried out for the parameter $r$ ranging between 1.3 and 1.9 which covers the region relevant for most polymers.

Table 2: Speed-up factors of the asymptotic expansion compared to the direct solution of the nonlinear two-scale Stokes problem. The execution time of the nonlinear two-scale problem is scaled to 1. In reality it is of the order of 1 minute on the fine mesh of the isotropic cell with $r = 1.3$ up to 193 minutes on the fine mesh of the anisotropic cell with $r = 1.3$ (1.8GHz Athlon, 1.5GB Memory, FEMLAB 2.3). Missing results ('—') indicate, that the direct solution method did not converge.

| | Isotropic cell | | | Anisotropic cell | | |
|---|---|---|---|---|---|---|
| $r$ | coarse | medium | fine | coarse | medium | fine |
| 1.3 | 1.95 | 1.58 | 1.51 | — | — | 1.58 |
| 1.5 | 1.52 | 1.70 | 1.51 | — | 1.53 | 2.30 |
| 1.7 | 1.50 | 1.35 | 1.36 | 3.54 | 1.52 | 1.53 |
| 1.9 | 1.52 | 1.69 | 1.95 | 2.88 | 1.73 | 3.79 |

In order to illustrate the accuracy, we show in Figure 3(left) the relative error between the "exact" solution $\boldsymbol{u}$ and the solution using the asymptotic expansion $\tilde{\boldsymbol{u}}$. The relative error is given by

$$E_R(\boldsymbol{y}) = \frac{\|\boldsymbol{u}(\boldsymbol{y}) - \tilde{\boldsymbol{u}}(\boldsymbol{y})\|_2}{\max\limits_{\boldsymbol{y}\in\mathcal{Y}} \|\boldsymbol{u}(\boldsymbol{y})\|_2} \,. \tag{24}$$

From a practical point of view, using an absolute norm, e.g. the error in the flow rate as one of the referees suggested, might be more appealing, since it directly shows the implications of the used asymptotics to the predicted productivity of the oil reservoir. However, since we are mainly interested in the applicability of the proposed ansatz, we focus on a relative norm based on the primary variables of the problem. In addition to the relative error in the velocity field, Figure 5 provides a comparison of the shear-rates and viscosities in the exact solution and the asymptotic one.

In case of isotropic media, the maximum of the relative error is about 4.5% and appears on the horizontal cell boundaries, whereas the relative error is smallest close to the surface of the obstacle.

Figure 3(right) shows the horizontal velocity component along the line $y_1 = 0.7$, $y_2 \in [0, 1]$ for $r = 1.3$. Again, the same behavior as in Figure 3(left) is clearly visible; the error is smallest close to the obstacle (here for $y_2 \approx 0.5$) and increases toward the boundaries. A close agreement between the "exact" solution and the asymptotic expansion is found. The solution using a Newtonian viscosity differs already quite significantly from the "exact" one, indicating the need of the correction terms introduced by the asymptotic expansion.

Analogously to the isotropic case, we consider the complex geometry shown in Figure 2(right). Again, the simulations are carried out for the parameter $r$ ranging between 1.3 and 1.9 and we compare the "exact" and the asymptotic solution. Due to the complexity of the geometry, the maximal relative errors are larger in the anisotropic case and reach about 10% on the finest triangulation.

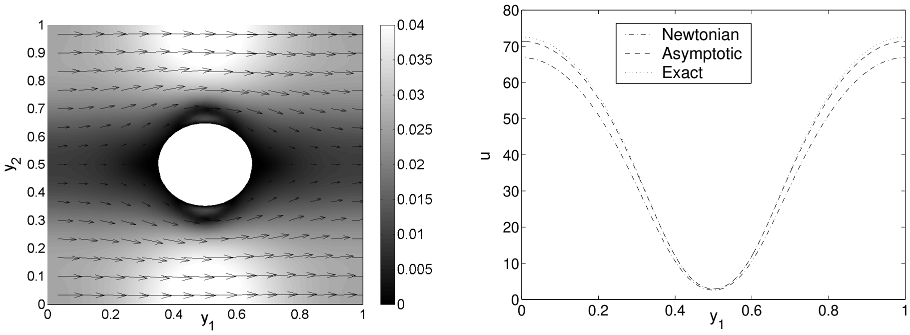


Figure 3: (left): Relative error $E_R(\boldsymbol{y})$ between "exact" solution and asymptotic expansion. The arrows visualize $\boldsymbol{u}(\boldsymbol{y}) - \tilde{\boldsymbol{u}}(\boldsymbol{y})$ and the greyscale shows the magnitude of the relative error. Computed on the fine grid.
(right): Velocity profile for $r = 1.3$ along the line $y_1 = 0.7$, $y_2 \in [0, 1]$. Note that the asymptotic solution ('– –') agrees very well with the "exact" solution ('. . . ').

In Figure 4(left) the relative error for $r = 1.5$ is shown and Figure 4(right) provides a comparison of the velocity profiles analogously to the isotropic geometry.

In Table 3 we list the relative errors for the isotropic and the anisotropic cell for the different triangulations and various values of the parameter $r$.

Table 3: Maximal relative errors for the two cell geometries, refined triangulations and various values of $r$. Missing results ('—') indicate, that the direct solution method did not converge.

| | Isotropic cell | | | Anisotropic cell | | |
|---|---|---|---|---|---|---|
| $r$ | coarse | medium | fine | coarse | medium | fine |
| 1.3 | 4.42% | 4.44% | 4.41% | — | — | 8.50% |
| 1.5 | 2.46% | 2.41% | 2.36% | — | 15.93% | 9.96% |
| 1.7 | 2.28% | 2.32% | 2.21% | 11.66% | 9.89% | 8.32% |
| 1.9 | 0.98% | 1.01% | 0.95% | 6.08% | 3.99% | 3.96% |

For the isotropic geometry the relative errors are independent of the used triangulation, whereas in the anisotropic case the errors depend on the grid. The direct solution of the two-scale problem did only converge on the finest triangulation for the anisotropic geometry case and $r = 1.3$. For $r = 1.5$ the direct solution converged already on the medium grid. Due to the non-linearity in the viscosity, small spatial stepsizes are needed in these cases. However, the asymptotic expansion converged on all grids, since it only requires the solution of a linear Stokes equation.

As to be expected, the errors are largest in the non-Newtonian regime, i. e. for

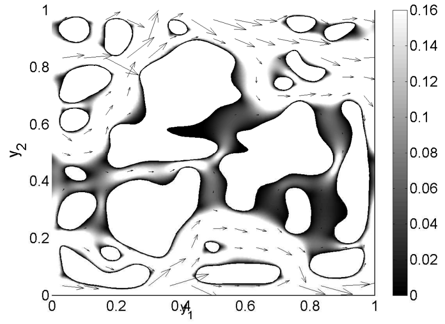


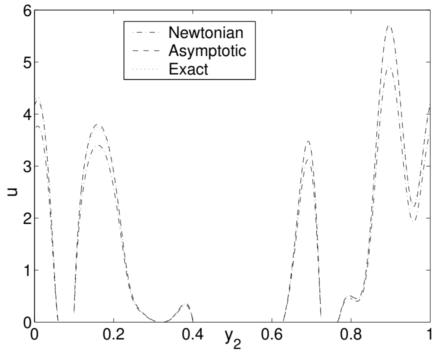


Figure 4: (left): Relative error $E_R(\boldsymbol{y})$ between "exact" solution and asymptotic expansion. The arrows visualize $\boldsymbol{u}(\boldsymbol{y}) - \tilde{\boldsymbol{u}}(\boldsymbol{y})$ and the greyscale shows the magnitude of the relative error. Computed for $r = 1.5$ on the medium grid.
(right): Velocity profile for $r = 1.3$ along the line $y_1 = 0.7$, $y_2 \in [0, 1]$ computed on the medium grid. Note, that the asymptotic solution ('– –') agrees perfectly wit the exact one ('. . . ').

$r = 1.3$ and decrease towards the Newtonian regime, i. e. for $r$ increasing for both geometries.

In Figure 5, the shear rates and the resulting nondimensional viscosities are shown for the "exact" and the asymptotic solution. For a given dimensionless $\lambda = 9 \times 10^{-6}$ and $r = 1.3$ we solve the two-scale and the asymptotic problem on the isotropic geometry. Using (19), the magnitude of the shear-rate is given by $\|D(\boldsymbol{u}_0)\|_2^2 = (\partial_k\, p_0)^2\ \|D(\boldsymbol{w}_k(\boldsymbol{y}))\|_2^2$. It is clearly visible from Figure 5(left), that the shear-rates are large but still $\lambda\, \|D(\boldsymbol{u}_0)\|_2^2 < 1$ holds. Figure 5(right) shows the computed viscosities; the viscosity determined by the asymptotic expansion agrees remarkably well with the "exact" viscosity.

### 4.3.2 Higher-Order Approximations

We have seen in the previous section that the relative errors in the isotropic case are independent of the grids. Hence the relative errors depend solely on the asymptotic expansion with respect to the parameter $\lambda$. To analyze the accuracy of the asymptotic method we consider the expansion up to the third order for the isotropic case on the coarse grid. We choose $r = 1.3$ because in this regime the nonlinearity is dominant and we vary the values of $\lambda$ between $9 \times 10^{-9}$ and $9 \times 10^{-6}$.

Figure 6 shows a log-log-plot of the maximum relative error versus the scaled expansion parameter $\lambda$. We observe two different regions, where the errors show different behaviors. Note, that the behaviors of errors change around $\lambda = 5.4 \times 10^{-7}$, which is found numerically. Hence we choose $\lambda = 5.4 \times 10^{-7}$ as a critical value which divides the errors into two regions. The first region covers the parameters $9 \times 10^{-9} \le \lambda < 5.4 \times 10^{-7}$ and the second region is

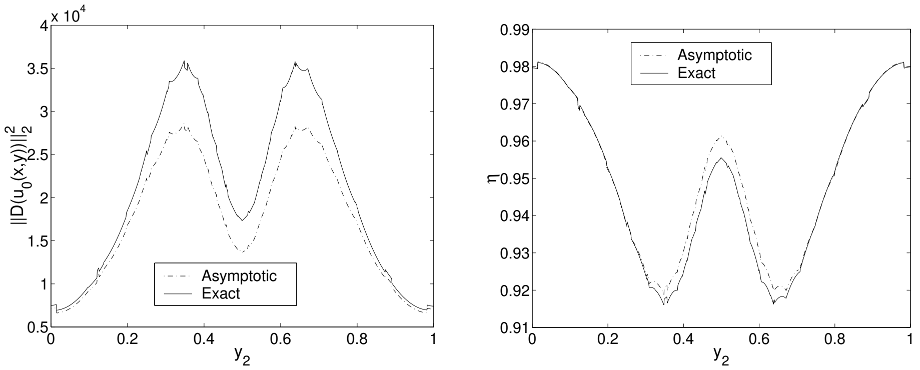


Figure 5: (left): Two-scale shear rate profile along the line $y_1 = 0.7$, $y_2 \in [0,1]$ for the isotropic case computed using the zeroth-order cell problem to get $\|D(w_k(y))\|_2^2$ and multiplied by the $(\partial_k\, p_0)^2$ for the asymptotic profile.
(right): Viscosity profile for isotropic case along the line $y_1 = 0.7$, $y_2 \in [0,1]$ computed on the medium grid.

$5.4 \times 10^{-7} \leq \lambda < 9 \times 10^{-6}$.

The figure 7 focuses on these two regions. A least-squares method was used to fit a linear function to the data. The slope of this linear fit yields the order of the error.

Table 4 lists the obtained orders of the error in the different regions.

Table 4: Computed orders of the approximation error in the two regions.

| | Approximation Order | | |
|---|---|---|---|
| Region | 1 | 2 | 3 |
| I | 0.99 | 0.92 | 0.90 |
| II | 0.84 | 2.02 | 2.56 |

In the first region shown in Figure 7(left), the order of the error is almost equal to 1, independent of the approximation order. Although $\lambda$ is rather small in this region, the change of the approximation seems not to be caused by a loss of significant figures in the computations. In the second region, see Figure 7(right), the error behaves almost as to be expected. The error for the first order approximation depends nearly linear on the expansion parameter $\lambda$ and for the second order expansion the error increases quadratically with $\lambda$. The deviation for the third order expansion might be caused by the numerical method.

At the moment we do not have a conclusive explanation for the existence of the two regions with different error behavior. Further investigations on this topic seem to be necessary.

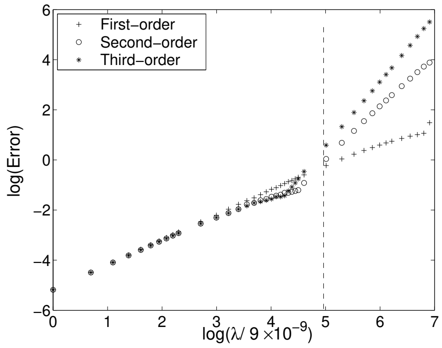


Figure 6: Correlation between the logarithm of $\lambda/9.0\times10^{-9}$ and the logarithm of the maximum relative error. The vertical dashed line separates the two regions of different error behavior.

# 5 Conclusions

An asymptotic expansion for the two-scale porous media flow equations with respect to small rheologic scale parameters has been presented. In the case of uni-directional pressure gradients we derived auxiliary problems decoupling the micro- and macrovariables. Finite element calculations were used to validate the proposed approach and for comparison with the solution of the non-linear two-scale problem.

For different pore geometries and various rheological parameters we found a remarkable good agreement between the asymptotic and the direct solution.

The relative errors introduced by the first-order asymptotic expansion are less than 5% in case of the isotropic and less than 10% in case of the anisotropic geometry on the fine grid. The speed-up factor of the asymptotic expansion was found to vary between 1.5 and 3.5 depending on the used grid, geometry and data. Higher-order expansions were studied in the isotropic case for various values of $\lambda$ with $r = 1.3$.

# Acknowledgements

The research of H. A. Parhusip was partly supported by a grant from the DAAD (German Academic Exchange Service, (code *A/00/41574*)) and partly by a grant from The Abdus Salam ICTP, Trieste (code *STEP-02/01*).

The authors also want to thank the referees for their useful comments and valuable suggestions.

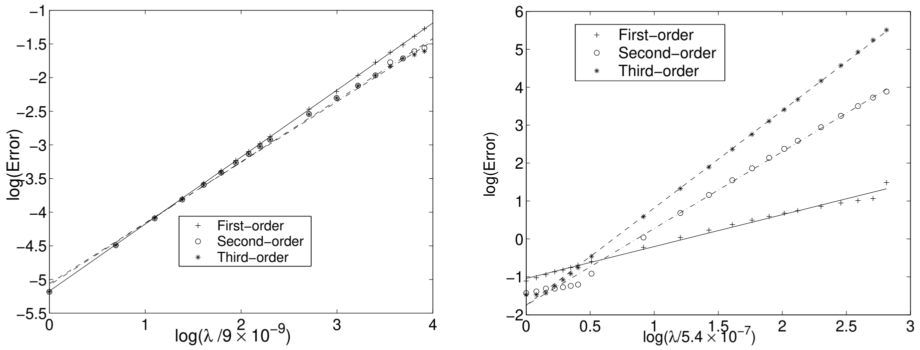


Figure 7: (left): Correlation between the logarithm of $\lambda/9.0\times10^{-9}$ and the logarithm of the maximum relative error for the region $9.0\times10^{-9}\le\lambda<5.40\times10^{-7}$. The solid line is the linear fit for the first-order approximation, the dash-dotted line for the second-order and the dashed line for the third-order approximation.
(right): Same results as in the left figure for region II: $5.40\times10^{-7}\le\lambda<9.0\times10^{-6}$.

# References


[1] K. S. Sorbie and D. Phil, *Polymer Improved Oil Recovery.* Glasgow: Blakie (1991) 359pp.

[2] A. Bartelds, *The Influence of Inaccessible and Excluded Pore Volume on Polymer Flooding.* PhD thesis, Delft University of Technology, 1998.

[3] M. London, IRIS Explorer in Oil Recovery, *Visualization Development Environments Proceedings* 2000.

[4] T. W. Patzek and D. B. Silin, Water Injection into a Low-Permeability Rock – 1: Hydrofracture Growth. *Transport in Porous Media*, 43 (2001) 537–555.

[5] G. Q. Tang and A. Firoozabadi, Effect of Pressure Gradient and Initial Water Saturation on Water Injection in Water-Wet and Mixed-Wet Fractured Porous Media. *SPE Reservoir Evaluation and Engineering*, (2001) 516–524.

[6] R. B. Bird, R. C. Armstrong, and O. Hassager, *Dynamics of Polymeric Liquids*, volume 1. New York: Wiley (1977) 649pp.

[7] K. S. Sorbie, P. J. Clifford, and E. R. W. Jones, The rheology of pseudoplastic fluids in porous media using network modeling. *Journal of Colloid and Interface Science* 130 (1989) 510–534.

[8] K. S. Sorbie and Y. Huang, Rheological and transport effects in the flow of low concentration xanthan solution through porous media. *Journal of Colloid and Interface Science* 145 (1991) 75–87.

[9] A. Koponen, M. Kataja, and J. Timonen, Simulations of single-fluid flow in porous media. *International Journal of Modern Physics C* 9 (1997) 1505–1521.

[10] U. Hornung, *Homogenization and Porous Media*. New York: Springer (1997) 279pp.

[11] A. Y. Beliaev and S. M. Kozlov, Darcy equation for random porous media. *Comm. Pure Appl. Math* 49 (1996) 1–34.

[12] A. Mikelic and I. Aganovic, Homogenization of stationary flow of miscible fluids in a domain with a grained boundary. *SIAM Journal Mathematical Analysis* 19 (1988) 287–294.

[13] G. Allaire, Homogenization of the Stokes flow in a connected porous medium. *Asymptotic Analysis* 2 (1989) 203–222.

[14] A. Bourgeat and A. Mikelic, Homogenization of a polymer flow through a porous medium. *Nonlinear Analysis, Theory, Methods and Applications* 26 (1996) 1221–1253.

[15] A. Mikelic, Homogenization theory and applications to filtration through porous media. In: A. Fasano (ed.), *Filtration in porous media and industrial application* (2000) 127–214.

[16] O. Gipouloux and Z. Abdel-Malek, Computation of the filtration laws through porous media for a non-Newtonian fluid obeying the power law. *Computational Geosciences* 1 (1997) 127–153.

[17] B. Bang and D. Lukkasen, Application of homogenization theory related to Stokes flow in porous media. *Applications of Mathematics* 44 (1999) 309–319.

[18] E. Marusic-Paloka and A. Mikelic, The derivation of a nonlinear filtration law including the inertia effects via homogenization. *Nonlinear Anal., Theory Methods Appl.* 42A (2000) 97–137.

[19] G. I. Barenblatt, V. M. Entov and V. M. Ryzhik, *Theory of fluid flows through natural rocks.* Dordrecht: Kluwer (1990) 395pp.

[20] H. Begehr and R. P. Gilbert, Non-Newtonian Hele-Shaw flows in $n \geq 2$ dimensions. *Nonlinear Anal., Theory Methods Appl.* 11 (1987) 17–47.

[21] L. Kondic, P. Palffy-Muhoray and M. J. Shelley, Models of non-Newtonian Hele-Shaw flow. *Phys. Rev. E* 54, No. 5 (1996) 4536–4539.

[22] R. P. Gilbert and M. Fang, Nonlinear systems arising from nonisothermal, non-Newtonian Hele-Shaw flows in the presence of body forces and sources. *Math. Computer Modelling* 35 (2002) 1425–1444.

[23] A. Fadili, P. M. J. Tardy and J. R. A. Pearson, A 3D filtration law for power-law fluids in heterogeneous porous media. *J. Non-Newtonian Fluid Mech* 106 (2002) 121–146.

[24] M. Griebel, T. Dornseifer, and T. Neunhoeffer, *Numerical Simulation in Fluid Dynamics.* Philadelphia: SIAM (1998) 217pp.

[25] R. Hilfer, Transport and relaxation phenomena in porous media. *Adv. Chem. Phys* 92 (1996) 299–424.

[26] H. P. S. Siregar, *Characterisation rheologique des solutions aqueuses de polyacrylamide utilisees en recuperation assistee du petrole.* Ph.D. thesis, University of Bordeaux, France, (1980) 103pp.

[27] R. Glowinski, J. L. Lions, and R. Tremolieres, *Numerical Analysis of Variational Inequalities.* Amsterdam: North Holland (1981) 776pp.

[28] R. Glowinski, *Numerical Methods for Nonlinear Variational Problems.* New York: Springer (1984) 493pp.

[29] V. Sarin, *Efficient Iterative Methods for Saddle Point Problems.* Ph.D. thesis, University of Illinois at Urbana-Champaign , (1997) 76pp.

[30] M. H. Holmes, *Introduction to Perturbation Methods.* New York: Springer (1995) 337pp.